Boundary-Layer Meteorol
DOI 10.1007/s10546-009-9456-5

ARTICLE

Resolved Versus Parametrized Boundary-Layer Plumes. Part I: A Parametrization-Oriented Conditional Sampling in Large-Eddy Simulations

F. Couvreux · F. Hourdin · C. Rio

Received: 24 February 2009 / Accepted: 17 November 2009

Abstract A conditional sampling based on the combination of a passive tracer emitted at the surface and thermodynamic variables is proposed to characterise organized structures in large-eddy simulations of cloud-free and cloudy boundary layers. The sampling is evaluated against more traditional sampling of dry thermals or clouds. It enables the characterization of convective updrafts from the surface to the top of the boundary layer (or the top of cumulus clouds), describing in particular the transition from the sub-cloud to the cloud layer, and retrieves plume characteristics, entrainment and detrainment rates, variances and fluxes. This sampling is used to analyze the contribution of boundary-layer thermals to vertical fluxes and variances.

Keywords Coherent structures · Conditional sampling · Convective boundary layer · Large-eddy simulations · Mass-flux parametrization

1 Introduction

The organized patterns of turbulence in the convective boundary layer (CBL) have been recognized for a while, in particular by glider pilots (see Atkinson and Zhang (1996) for a review of the different organizations). Coherent structures are a key element of the CBL and participate strongly in the turbulent vertical transport of heat, momentum and trace species, via a non-local transport. In climate and weather forecast numerical models, these structures are not explicitly resolved and must be parametrized. To represent the various scales of turbulence within the CBL, a recently-introduced approach consists in combining an eddy-diffusivity scheme, traditionally used for the representation of turbulent eddies, and a mass-flux scheme, traditionally used for moist convection. This new approach is now accepted as an efficient

F. Couvreux (✉) · C. Rio
CNRM-GAME Meteo-France and CNRS, 42 av Coriolis, 31057 Toulouse, France
e-mail: fleur.couvreux@meteo.fr

F. Hourdin
LMD-IPSL, pl Jussieu, 75005 Paris, France

Published online: 11 December 2009

means of representing vertical mixing in the CBL (for example, Chatfield and Brost 1987; Siebesma and Teixeira 2000; Hourdin et al. 2002; Soares et al. 2004; Rio and Hourdin 2008; Siebesma et al. 2007; Pergaud et al. 2009). The mass-flux scheme accounts for the vertical transport by coherent structures in the CBL, viz. thermal plumes, cells or rolls.

CBL coherent structures have been studied extensively in recent decades. Their main characteristics, thermodynamic perturbations and coverage fraction have been investigated using aircraft turbulence measurements (Lenschow and Stephens 1980; Greenhut and Khalsa 1982; Young 1988). However, such observations only describe a few particular levels in the boundary layer. Recently, new instruments such as radars have been used to infer more globally the features of these structures: for example, Miao et al. (2006) provide information on the upper two-thirds of the boundary layer. Observations aside, large-eddy simulations (LES) that resolve explicitly any circulation with scales larger than 20–100 m have become a central tool for the understanding and quantification of convective and cloud processes, and provide full three-dimensional fields of various variables. They have been widely used for the study of clear and cloudy boundary layers and have been extensively validated in studies of the clear boundary layer (Schumann and Moeng 1991; Moeng and Sullivan 1994; Couvreux et al. 2005), and of non-precipitating cumulus clouds (Heus and Jonker 2008, among others).

Identification of coherent structures in observations and LES is difficult and still a critical issue (Lenschow et al. 1980; Lenschow and Stephens 1980; Crum et al. 1987; Williams and Hacker 1992; Miao et al. 2006) even though clouds are easier to isolate due to their visual appearance and their positive liquid water content attribute (Siebesma and Cuijpers 1995). Yet, characterizing the structures in the cloud-free and cloudy boundary layer is necessary in order to link LES and mass-flux parametrizations. This implies the definition of an adequate conditional sampling. The combination of three different criteria, as reviewed by Berg and Stull (2004), have been used to identify the updrafts: (i) an indicator variable to define the thermal, either θ_v, the virtual potential temperature, θ, the potential temperature, r, the water vapour mixing ratio, or w, the vertical velocity; (ii) a threshold value for this indicator variable (the standard deviation is commonly used, see e.g. Lenschow et al. (1980)); and (iii) a length scale that constrains the geometrical size of thermals. The samplings proposed so far in the literature have been restricted to a fraction of the boundary layer, either its lower part or the cloudy part. The objective of the present work is to identify a sampling that characterises the thermals from the surface to the top of the dry CBL, or the top of clouds in the cloudy CBL. Another decisive requirement for the selection of the sampling is that it should optimize the top-hat estimate of the turbulent fluxes.

The new conditional sampling distinguishes air arriving from the surface using an idealized tracer emitted at the ground. This new conditional sampling (denoted CS), by characterizing the organized bottom-up transport in the CBL, is proposed as a method to link LES and mass-flux parametrizations.

In the following, the conditional sampling is first presented; it is shown that this conditional sampling characterizes thermals from the surface to the top of clouds. The conditional sampling is applied to thermals in a cloud-free boundary layer and two cumulus cases in Sect. 3, and evaluated against observations and more traditional samplings. Sensitivity tests are eventually presented in order to assess the impact of the conditional sampling specification. A discussion on the contribution of coherent structures to fluxes and variances follows, which highlights the potential of such sampling to the understanding of physical processes in the CBL. A companion paper (Rio et al. 2010) uses this conditional sampling extensively to evaluate and improve the thermal plume model of Rio and Hourdin (2008), focusing on the representation of mixing rates.

2 A Conditional Sampling of Boundary-Layer Thermals

Here, we present the new conditional sampling and evaluate it against other conditional samplings. This sampling aims at selecting the convective updrafts, large columns of rising air in the convective mixed layer originating from the unstable surface layer.

2.1 Definition

In the dry convective boundary layer, coherent structures are traditionally characterized by considering variables such as total water vapour mixing ratio, virtual potential temperature or vertical velocity. In Berg and Stull (2004) several criteria have been compared (see their Table 1). The vertical velocity is not an appropriate variable to select coherent structures since turbulent fluctuations inside and outside thermals may be larger than the mean thermal updraft velocity as indicated in Lenschow and Stephens (1980) and shown in Williams and Hacker (1992) (their Figs. 4 and 5). In the lower part of the mixed layer, Williams and Hacker (1992) argue that the virtual potential temperature, the excess of which is the driver for the vertical motion of thermal plumes, satisfactorily characterizes the structures. However, as they mention, this variable only characterises thermals in the lower half of the mixed layer since the thermal buoyancy decreases significantly above. Lenschow and Stephens (1980), using aircraft observations over the ocean, were the first to propose water vapour mixing ratio (r) as an indicator of thermals, since it can also distinguish them in the upper part of the boundary layer due to the negative vertical humidity gradient. Crum et al. (1987) also show that r is the best criterion based on observations of thermals by aircraft and Lidar over land as this variable exhibits a 'top-hat' appearance. Grossman (1984) suggested that the use of both moisture and vertical velocity instead of a unique variable is more efficient in describing convective cell characteristics over ocean. But they only use these criteria to describe the lower part of the boundary layer, up to $0.25 z_i$ (z_i being the CBL height). Recently, Miao et al. (2006) used airborne radar measurements combined with aircraft flight level data to provide thermodynamic and vertical velocity characteristics of coherent structures under clear conditions up to $0.8 z_i$. Conditional samplings to characterize cumulus clouds have also been proposed, namely the 'cloud' (all non-zero liquid water content points) and 'core' (buoyant ascending and cloudy points) samplings defined by Siebesma and Cuijpers (1995). As indicated previously, there is a lack of a sampling that enables the characterization of coherent structures from the surface to the top of shallow cumulus; in particular, no sampling exists that characterizes the transition zone from the sub-cloud to the cloud layer. In addition, a fundamental requirement is that the sampling should allow optimization of the representation of turbulent fluxes carried by thermals. The new conditional sampling presented here is bivariate as in Grossman (1984) but uses a passive tracer emitted at the surface, instead of the water vapour mixing ratio. The tracer is emitted with a constant surface flux and undergoes radioactive decay with a time constant τ_o:

$$\frac{\partial C}{\partial t} = -\frac{C}{\tau_o}. \tag{1}$$

The conditional sampling is defined as follows:

$$x \in \text{CS if } sv' > m \times \max(\sigma_{sv}, \sigma_{\min}) \text{ and } w > 0, \tag{2}$$

where $sv'(w)$ is the tracer concentration (respectively the vertical velocity) anomaly, σ_{sv} is the standard deviation of the tracer concentration at a given vertical level, m is a scaling factor, and $\sigma_{\min}$, is a minimum threshold.

As in Berg and Stull (2004), the threshold is defined as proportional to the standard deviation of the tracer concentration. Using a threshold proportional to the standard deviation induces an automatic adaptation to the intensity of turbulence, and ensures a conditional sampling valid for many cases. A minimum threshold at a given altitude, z, $\sigma_{\min}(z)$, is introduced: $\sigma_{\min}(z) = (0.05/z)\int_0^z \sigma_{sv}(k)dk$. Its value of 5% of the average standard deviation at lower levels ensures that no point is selected in a non-turbulent environment where a standard deviation is still defined, as above the cloud layer. A null threshold is used for the vertical velocity, and the only constraint is that the parcel must be ascending. This conditional sampling is applied at each vertical level independently.

In the case of cumulus-topped thermals, the definition is applied up to $z = z_b + (z_t - z_b)/4$ where z_b and z_t stand for cloud base and cloud-top height. Above that level, a cloud condition ($ql > 0$ with ql the liquid water content) is added in order to select only cloudy grid points and not air that is detrained from the cloud:

$$\text{if z} \geq z_b + \frac{z_t - z_b}{4}, x \in \text{CS if } sv' > m \times \max(\sigma_{sv}, \sigma_{\min}) \text{ and } w > 0 \text{ and } ql > 0. \quad (3)$$

This is necessary when dissipating or mature clouds dominate, which have a larger portion of detrained air (Zhao and Austin 2005) still characterized by a positive anomaly of the tracer concentration and positive vertical velocity. Sensitivity to this addition is detailed in Sect. 4.5. An additional condition could be added on the horizontal length scale of the perturbations, as is often done for observations reported in the literature.

The conditional sampling uses an idealized tracer and is therefore not appropriate for an application to observations. It is developed in order to provide a new tool to evaluate CBL mass-flux parametrizations.

2.2 Large-Eddy Simulations

The large-eddy simulations used here have been performed with the LES version of the non-hydrostatic model Meso-NH (Lafore et al. 1998). The subgrid turbulence scheme is based on a prognostic equation of the turbulent kinetic energy using a Deardorff mixing-length scale (Cuxart et al. 2000). The LES model has a 100- or 50-m horizontal resolution and a stretched vertical resolution inferior to 50 m in the boundary layer (see details in Sects. 3.1 and 3.2 and for the different cases). Here the conditional averaging procedure is based solely on the resolved fields. The subgrid scheme contributes to less than 15% of total fluxes and variances except close to the surface (levels lower than 100 m). Sensitivity tests to the horizontal resolution are presented in Sect. 4.1. To reduce statistical errors, results are averaged over a time period varying for the different cases (30 min for the stationary case, 10 min for the diurnal cycle cases) with 1-min sampling.

In practice, two tracers are introduced with a time constant τ_o (Eq. 1) of 15 min for tracer sv or 60 min for tracer sv_2. For the three cases considered in the following, the characteristic time scale of the dry or sub-cloud boundary layer, defined by $T = z_i/w_*$ (with z_i the boundary-layer height and w_* the convective velocity scale) ranges from 9 min (for a cloud-free continental CBL case) to 16 min (for an oceanic trade-wind cumulus case).

2.3 Conditional Sampling Characteristics

Figure 1 shows the part of the tracer concentration distribution selected by this conditional sampling (shaded area, Eqs. 2, 3 with $m = 1$) at different heights, from the near surface

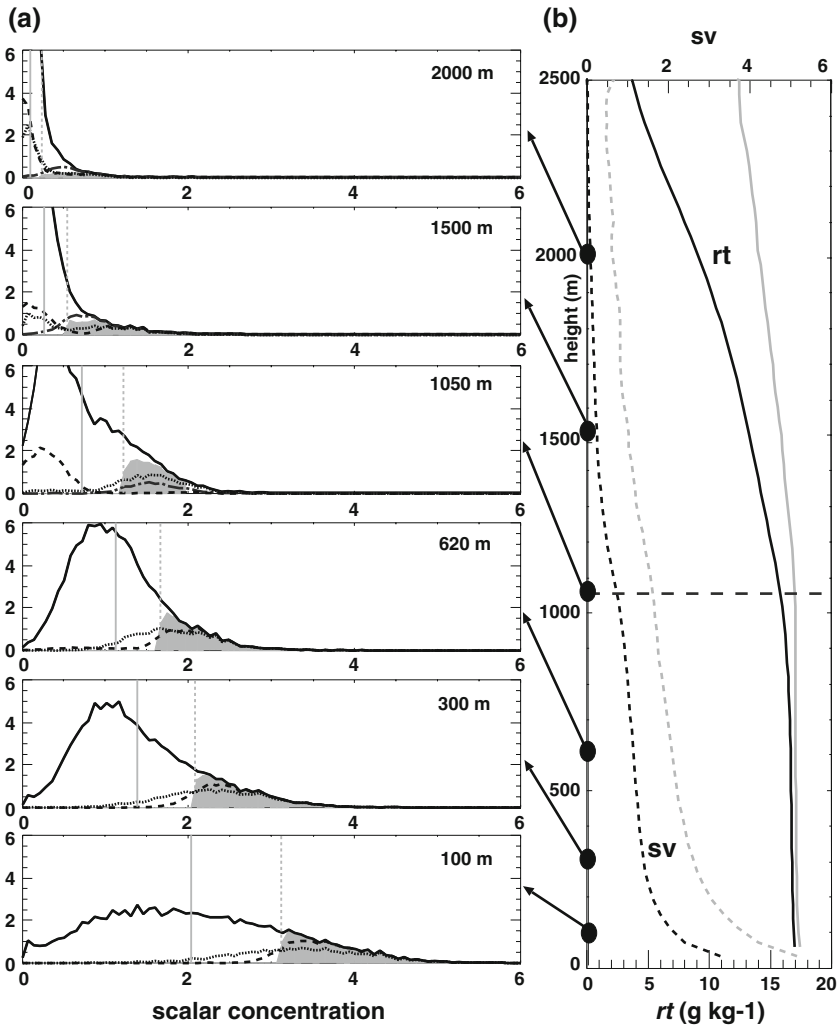

Fig. 1 **a** Distribution of the tracer concentration in the sub-cloud and cloud layers for ARM 1430 LT. The *full line* corresponds to the distribution of the tracer concentration, the *dotted line* to the part of the distribution selected by $w' > \sigma_w$, the *dashed line* to the part of the distribution selected by $\theta_v' > \sigma_{\theta_v}$, the *shaded area* to the part of the distribution selected by the CS. The *thick dash-dot dark grey line* corresponds to the part of the distribution selected by the cloud sampling (all non-zero liquid water content points). The *vertical grey full and dotted lines* correspond respectively to the mean value and the mean plus standard deviation of the tracer concentration. **b** Vertical profiles of the total water vapour mixing ratio (*full lines*) and the tracer concentration (*dashed lines*) averaged over the whole domain (*black*) or over the CS (*grey*). The *horizontal dashed line* indicates the cloud base height

(100 m) to the upper part of the cloud layer for a continental cumulus case (from the Atmospheric Radiation Measurement (ARM) in the following, 1430 local time (LT), see below for details on this case). The part of the tracer concentration distribution selected by other conditional samplings (using the vertical velocity, the virtual potential temperature or the liquid water content) is also shown. As expected, in the lower half of the boundary layer the sampling

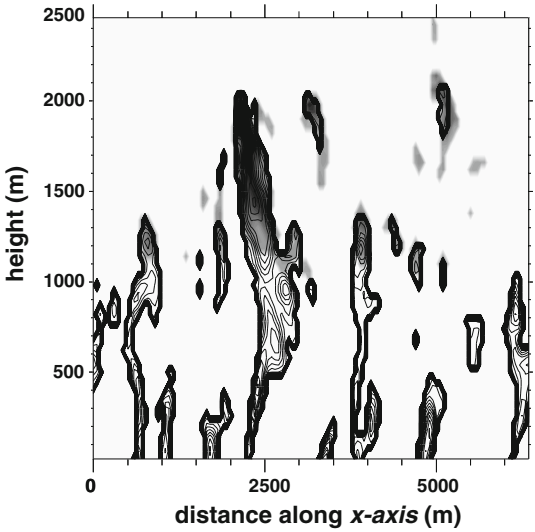

Fig. 2 Example of vertical cross-section in the 3D domain of the selection achieved by the CS (*thick contours*) for ARM 1430 LT. The *thin lines* correspond to the tracer concentration among the CS structures. The *shaded area* indicates clouds ($ql > 0$)

selects the moister (not shown), most buoyant and the fastest rising points. Buoyancy and tracer based samplings are similar in that region. The vertical velocity sampling also selects points with lower tracer concentration due to the highly perturbed (by small-scale turbulence) nature of the vertical velocity: this sampling does not necessarily select coherent structures, in agreement with Lenschow and Stephens (1980). Almost all the points with $sv' > \sigma_{sv}$ (to the right-hand side of the vertical dashed line) are selected in the lower levels, showing the weak role of the vertical velocity condition. In the upper part of the sub-cloud layer, more highly buoyant points are discarded as the coherent structures progressively acquire negative buoyancy, the environment becoming warmer due to entrainment at the inversion layer. This behaviour is amplified at higher levels.

At cloud base, the use of the vertical velocity in the conditional sampling modifies the selection and this is enhanced when reaching deeper cloud levels. This is mainly due to cloudy downdrafts (about 20% of the cloud cover) that are not selected by the conditional sampling if the vertical velocity is also used as a constraint. In the first 200 m of the cloud layer, about half of the selected points are not cloudy corresponding to overshooting thermals that do not condensate. Above, not all the cloudy grid points are selected, but this sampling is intermediate between the cloud and the core sampling. In fact, the small grey area reflects the small cloud fraction in cumulus cases (about 5% in that case).

To sum-up, the conditional sampling is similar to the buoyancy sampling in the lower part of the CBL and to the cloud sampling in the upper part of the cloud layer. Moreover it characterizes thermals from the surface to the top of clouds, providing a description of the transition from the sub-cloud to the cloud layer. Figure 2 illustrates the vertical consistency of the selection by this sampling (grey shaded zone) even though the conditional sampling is applied independently at each vertical level. A visible link between thermals and clouds is apparent, thermals consisting of the roots of clouds in agreement with LeMone and Pennell (1976).

As shown later (see Sect. 4.6), an additional advantage of this sampling is to maximize the contribution to fluxes and variances among the different traditional samplings.

3 Characteristics of Coherent Structures in LES

In this section, we evaluate the conditional sampling in three cases: a cloud-free CBL, a trade-wind cumulus case, and a case of shallow convection diurnal cycle over land.

3.1 Characteristics of Organized Structures in a Cloud-Free CBL

This case is based on observations from the International H20 project, IHOP (Weckwerth et al. 2004) and designed to represent a mostly clear growing boundary layer over land with light winds. It focuses on the diurnal development of the boundary layer from early morning to early afternoon of 14 June 2002, where the sensible and latent heat fluxes reach 200 and $170\,\mathrm{W\,m^{-2}}$ respectively. The LES domain is $10 \times 10 \times 4\,\mathrm{km}^3$, the horizontal resolution is 100 m and the vertical resolution is stretched and finer than 50 m in the whole boundary layer. The simulation has been documented and extensively evaluated with IHOP observations (Couvreux et al. 2005).

For this particular case, structure characteristics obtained through the conditional sampling can be directly compared to values deduced from aircraft in-situ measurements where organized structures have been identified on airborne radar reflectivity, 'echo plumes', or airborne Doppler velocity, 'updraft plumes' (Miao et al. 2006). Their sampling, based on radar observations, presents similarities with the present tracer-based conditional sampling since the reflectivity is thought to be due to the higher density of insects that can be viewed as a surface tracer. These observations were recorded during three clear days of the IHOP between 1300 and 1600 LT, representative of thermal features over the Southern Great Plains for a clear boundary layer. Therefore they can be compared to the IHOP simulation.

Figure 3 illustrates such a comparison for the r, θ, θ_v and w perturbations of coherent structures. Normalized vertical profiles are consistent between observations and the conditional sampling for the IHOP simulations. Results also agree with the similarity laws of Lenschow and Stephens (1980) (triangles) at least in the lower half of the CBL for the thermodynamical variables. There are discrepancies in the vertical velocity profiles, in particular regarding the height of the maximum. Note that the similarity laws of Sorbjan (1986) agree more with the LES results, with a maximum of the vertical velocity anomaly near the middle of the boundary layer (not shown). In the upper half of the CBL, the similarity laws do not reproduce the moisture excess increase nor the temperature decrease with height due to entrainment of dry and warm air between plumes, a phenomenon highlighted by Couvreux et al. (2007). Thermals are buoyant up to $0.85z_i$, slightly higher than in the observations and than in Young (1988). They also acquire a negative potential temperature anomaly at $0.8z_i$ in agreement with observations, and have a maximum of vertical velocity near the middle of the boundary layer (a lower maximum, at $0.33z_i$, is noted when a less restrictive sampling is used by Young (1988)). The vertical velocity decreases more rapidly with height above $0.5z_i$ in the observations than in the simulations, and is partly due to the addition of a condition on the vertical velocity (see differences between the grey full and dotted lines). This condition only significantly modifies the results in the upper part of the boundary layer (Fig. 3). The fractional coverage (not shown) is almost constant with height (slightly decreasing), varying from 0.2 to 0.13 in agreement with the 0.2 value found by Miao et al. (2006). This is consistent with results of Young (1988) even though he found a larger coverage due to a less restrictive threshold. Therefore, the thermodynamic characteristics of dry thermals are well reproduced with the conditional sampling.

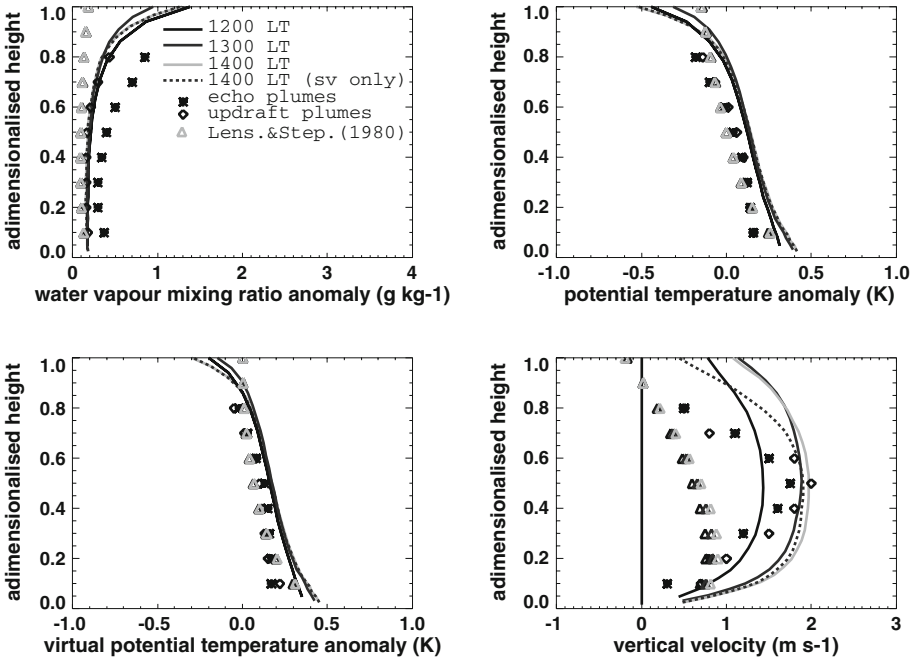

Fig. 3 Normalized vertical profiles of thermodynamic (water vapour mixing ratio, potential temperature, virtual potential temperature and vertical velocity) perturbations of coherent structures in the clear boundary-layer derived from the CS for IHOP-2002 simulation (1200 LT in *black*, 1300 LT in *dark grey* and 1400 LT hour in *light grey*) or from echo plumes (*stars*) and updraft plumes (*diamonds*) of Miao et al. (2006) (values deduced from aircraft in-situ measurements where organized structures have been identified on airborne radar reflectivity). The conditional sampling based only on the tracer (no constraint on the vertical velocity) is indicated by *dotted lines* for IHOP, 1400 LT. The *triangles* correspond to the similarity laws of Lenschow and Stephens (1980)

3.2 Characteristics of Coherent Structures in the Cloudy Boundary Layer

The conditional sampling is evaluated against the traditional cloud and core samplings proposed by Siebesma and Cuijpers (1995) in the cloud layer for two cumulus cases.

The first case represents an oceanic cloudy boundary layer derived from the Barbados Oceanographic Meteorological Experiment (BOMEX) and described in Siebesma et al. (2003). For this case, the surface sensible and latent heat fluxes are constant and equal to 8 and 150 W m^{-2} respectively. The cloud base is located at about 500 m and cloud top at about 2000 m; 6 h are simulated and the first 3 h are discarded as spin-up.

The second case represents a growing continental boundary layer derived from the Southern Great Plains ARM site and described in Brown et al. (2002). It focuses on the diurnal cycle of shallow convection, with the sensible and latent heat fluxes reaching 140 and 500 W m^{-2} respectively. Fifteen hours are simulated. In this case, clouds are initiated at 0930 LT (the fourth hour) and dissipate at 1830 LT. We therefore focus on the period 1030 to 1730 LT: cloud base ranges from 800 to 1200 m and cloud top from 1100 to 2700 m in this time period. Both simulations have the same horizontal domain, 6.4 $\times$ 6.4 km^2, and a larger vertical domain for ARM (4 km) than for BOMEX (3 km). The horizontal resolution, 50 m, is finer than that used in Siebesma et al. (2003), and the vertical resolution, 40 m, is similar.

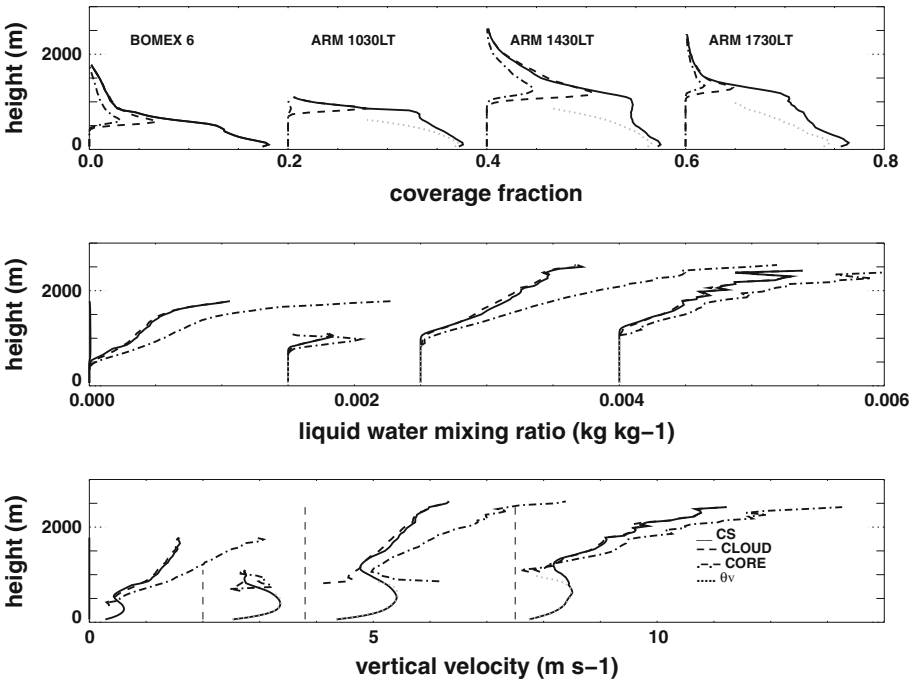

Fig. 4 Vertical profiles of the coverage fraction (*upper panel*), liquid water mixing ratio ($\mathrm{kg\,kg^{-1}}$, *middle panel*), vertical velocity ($\mathrm{m\,s^{-1}}$, *lower panel*) for BOMEX sixth hour (*left profiles*), ARM 1030 LT (*middle left profiles*, translated to the right by respectively 0.2, $0.0015\,\mathrm{kg\,kg^{-1}}$ and $2\,\mathrm{m\,s^{-1}}$ for the different graphs), 1430 LT (*middle right profiles*, translated by 0.4, $0.0025\,\mathrm{kg\,kg^{-1}}$ and $3.5\,\mathrm{m\,s^{-1}}$) and 1730 LT (*right profiles*, translated by 0.6, $0.004\,\mathrm{kg\,kg^{-1}}$ and $5\,\mathrm{m\,s^{-1}}$) for the CS (*full line*), the cloud (*dashed line*) and core (*dot-dashed line*) samplings. The virtual potential temperature sampling ($\theta_v' > \sigma_{\theta_v}$ and $w > 0$) is also overplotted up to $0.8z_i$ for ARM hours in *grey dotted lines*

As proposed by Nicholls and LeMone (1980), the same thermodynamic properties as in the dry boundary layer hold for the sub-cloud layer for these two cases. Figure 4 illustrates, for ARM hours, that the conditional sampling is consistent with results of more traditional samplings for the sub-cloud layer such as the θ_v sampling (dotted lines) up to $0.8z_i$.

Figure 4 shows a comparison of the conditional sampling with the cloud and core samplings for the coverage fraction, the liquid water content and the vertical velocity for BOMEX, sixth hour, and for ARM, 1030, 1430 and 1730 LT. Thermodynamic perturbations are intermediate between the cloud and the core samplings but match more with the cloud sampling as illustrated for the liquid water content or the vertical velocity. The sampling coverage is also very close to the cloud fraction. No discontinuity is noted at $z = z_b + (z_t - z_b)/4$ where a condition on the liquid water content is added. The coverage fraction in the cloud layer is in agreement with observations, where typical values of 3–5% are reported by Albrecht (1981).

These three cases illustrate that conditional sampling is similar to the buoyancy sampling in the lower part of the boundary layer and to cloud sampling in the cloud layer. Moreover, it continuously characterizes updrafts from the surface to the cloud top.

4 Sensitivity Tests

Sensitivity tests are conducted in order to assess the impact of the chosen criteria. They are presented for ARM at 1430 LT where the cloud layer has its deepest extension. But similar results hold for other hours in ARM, BOMEX and IHOP. Figures 5, 6 and 7 show the implications of the sensitivity tests for the coverage fraction and the vertical velocity. In this section, it is also demonstrated that the conditional sampling maximizes the contribution to the liquid potential temperature flux and the total moisture flux.

4.1 Sensitivity to the Horizontal Resolution

To evaluate the sensitivity to the horizontal resolution, the reference simulation is compared to one with a coarser grid (100 m, as in the intercomparison, instead of 50 m). As shown in Fig. 5 (a and b, black full and dash-dot lines), characteristics of the updrafts are similar with less than 10% of differences. No systematic bias exists. Therefore, in the following, the various sensitivity tests are performed with a 100-m resolution. Nevertheless, as differences increase when analyzing fluxes and variances, the contribution to the vertical transport is analyzed with the high-resolution simulations.

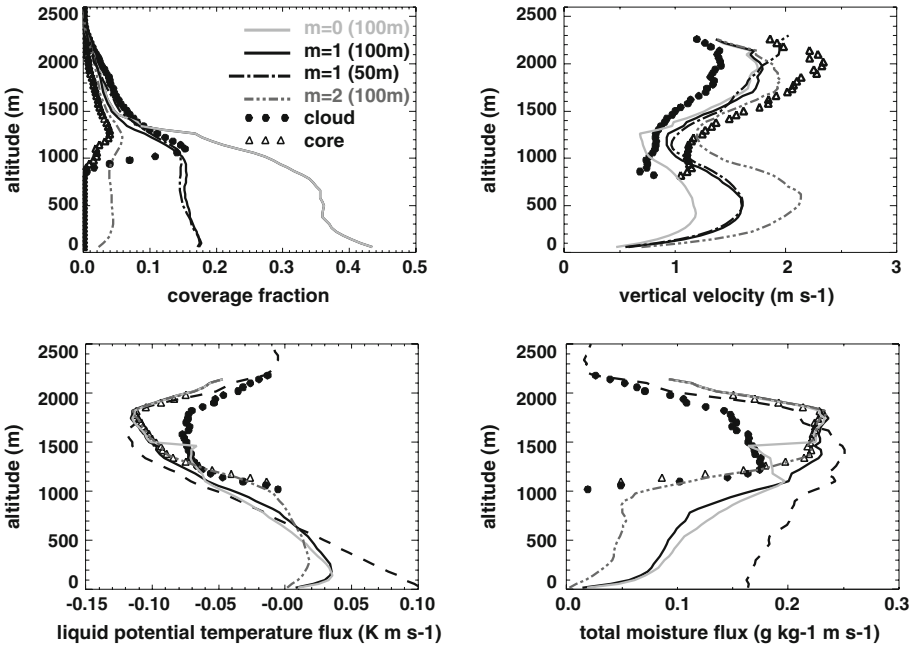

Fig. 5 Vertical profiles of the coverage fraction, the vertical velocity ($\mathrm{m\,s^{-1}}$) the liquid potential temperature flux ($\mathrm{K\,m\,s^{-1}}$) and the total water vapour mixing ratio flux ($\mathrm{g\,kg^{-1}\,m\,s^{-1}}$) for ARM 1430 LT for samplings with various thresholds: $m = 0$ (*black grey*), $m = 1$ (*black*), $m = 2$ (*dark grey dash-dot-dot line*). The *dash-dotted line* corresponds to the simulation with the fine (50 m) resolution and $m = 1$. The cloud (*full circles*) and core (*triangles*) samplings are also indicated for information. For the *bottom panels*, the *long-dashed black line* indicates the total flux and the simulations with lower resolution are omitted

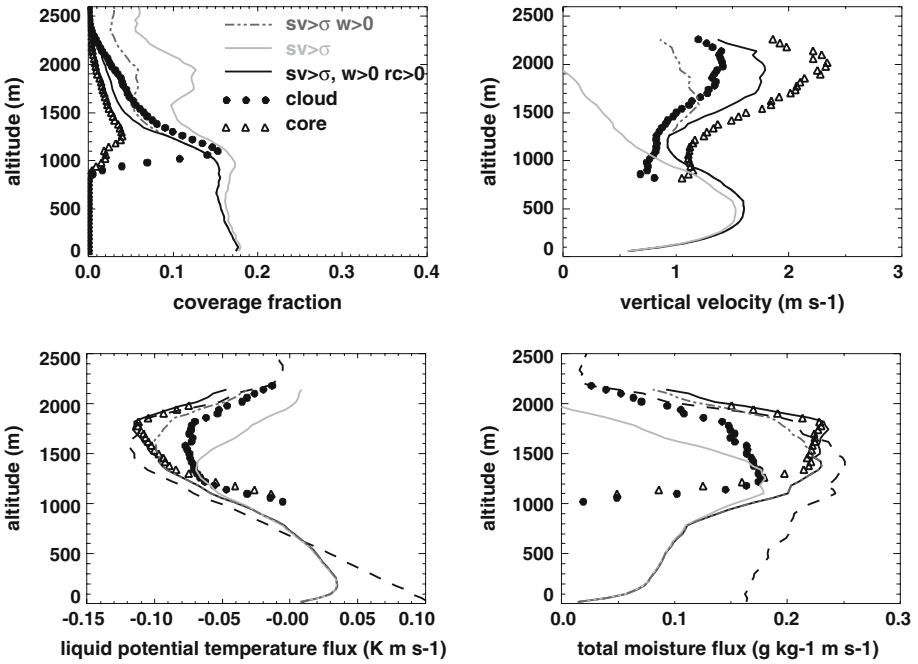

Fig. 6 Vertical profiles of the coverage fraction, the vertical velocity (m s^{-1}), the liquid potential temperature flux (K m s^{-1}) and the total water vapour mixing ratio flux (g kg^{-1} m s^{-1}) for ARM 1430 LT for the following samplings: $sv' > \sigma_{sv}$ (*light grey line*), $sv' > \sigma_{sv}$ and $w > 0$ (*dark grey dash-dot-dotted line*), $sv' > \sigma_{sv}$ and $w > 0$ and $ql > 0$ (*black*). The cloud (*full circles*) and core (*triangles*) samplings are also indicated for information. For the *bottom panels*, the *long-dashed black line* indicates the total flux

4.2 Sensitivity to the Threshold

Figure 5 also shows that results are highly sensitive to the threshold, especially for the coverage fraction. Taking $m = 2$ in Eq. 2 induces a reduction of the coverage fraction from 0.17 to 0.05 in the sub-cloud layer. The effect is weaker in the cloud layer. As expected perturbations of the structures relative to the environment are enlarged (variations of up to 0.1–0.2 K for θ_l and θ_v, 0.5 m s^{-1} for w and 0.25 g kg^{-1} for r_t, the total water vapour mixing ratio, compared to the reference threshold), nevertheless the shape of the vertical profiles is unchanged (Fig. 5). Taking $m = 2$ also reduces the contribution to the liquid potential temperature and total moisture flux, while taking $m = 0$ leads to a larger coverage fraction and smaller perturbations. Note the discontinuity in the contribution to the liquid potential temperature and the total moisture flux at $z = z_b + (z_t - z_b)/4$ indicating the inconsistency between the definition below and above this height. Taking $m = 1$ gives consistent values of the fractional coverage with the fraction derived from observations (Sect. 3.1) for the IHOP case. A fraction ranging from 0.1 to 0.2 in the sub-cloud layer is also consistent with other observations, for example 0.16 in Greenhut and Khalsa (1982) using the vertical velocity with a standard deviation threshold. Moreover, $m = 1$ is the threshold that enables us to explain the largest contribution to the liquid potential temperature flux despite the relatively small coverage fraction (compared to $m = 0$). Therefore, in the following, $m = 1$ is used.

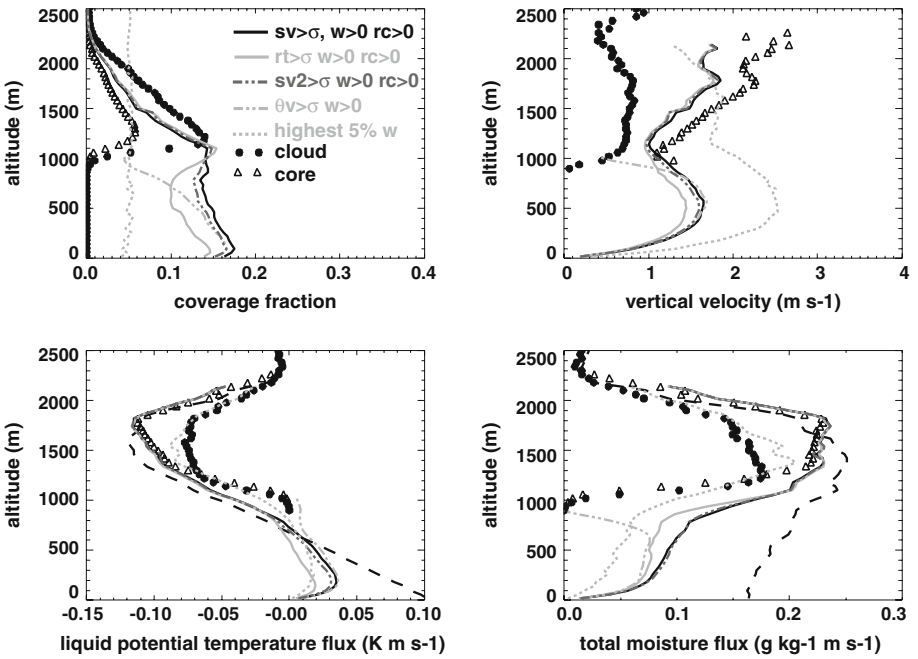

Fig. 7 Vertical profiles of the coverage fraction, the vertical velocity ($\mathrm{m\,s^{-1}}$) and the liquid potential temperature flux ($\mathrm{K\,m\,s^{-1}}$) and the total water vapour mixing ratio flux ($\mathrm{g\,kg^{-1}\,m\,s^{-1}}$) for ARM 1430 LT for different samplings: $sv' > \sigma_{sv}$ and $w > 0$ and $ql > 0$ (*black*), $r_t' > \sigma_{r_t}$ and $w > 0$ and $ql > 0$ (*light grey*), $sv_2' > \sigma_{sv_2}$ and $w > 0$ and $ql > 0$ (*dark grey dash-dot-dot line*), $\theta_v' > \sigma_{\theta_v}$ and $w > 0$ (up to $0.8z_i$, *light grey dash-dotted line*) and the 5% highest vertical velocities (*light grey dotted line*). The cloud (*full circles*) and core (*triangles*) samplings are also indicated for information. For the *bottom panels*, the *long-dashed black line* indicates the total flux

4.3 Sensitivity to the Spatial Filtering

We test here the effect of adding a condition on the horizontal continuity. In practice, we retain points only if the conditional sampling is satisfied uniformly over more than the chosen length scale in both horizontal directions. Here, a minimum length scale of 150 m is chosen instead of 50 m implied by the horizontal resolution. This addition induces a slightly smaller coverage fraction and slightly higher perturbations (not shown). The differences are mainly noted in the upper half of the cloud layer where the grid points with the largest tracer concentration are scattered with only part of them composed of groups of more than three points in both horizontal directions. Nevertheless, as in past studies, a minimum length scale of 50 m was mainly used (Williams and Hacker 1992, for example), consistent with the horizontal resolution of the simulation. In the following, no minimum size of the perturbations is imposed.

4.4 Sensitivity to the Additional Condition on the Vertical Velocity

The addition of a condition on the vertical velocity, ensuring that only ascending grid points are chosen, avoids the selection of air that is detrained and acquires negative vertical velocity, still characterized by a positive tracer concentration anomaly. The implication of an additional w condition is illustrated in Fig. 6 by a smaller coverage fraction (dark grey dash-dot-dotted

lines). This addition also induces a larger vertical velocity. The reduction of the fraction is progressive in the sub-cloud layer from a difference of 0.003 at the surface to a difference of 0.016 at the top of the boundary layer as expected with higher detrainment close to the top of the sub-cloud layer. This modification has no impact on the flux in the sub-cloud layer suggesting a compensation between the modification of the coverage fraction and of the vertical velocity. In the cloud layer, the difference of the coverage fraction ranges from 0.02 to 0.07. Downdrafts represent about 15–20% of cloudy parcels in the lower half of the cloud layer and 30–35% in the upper half. This is consistent with Zhao and Austin (2005), with more downdrafts in the upper part of clouds. Similarly, the condition on the vertical velocity excludes the subsiding shells (Heus and Jonker 2008).

4.5 Sensitivity to an Additional Condition on the Liquid Water Content

The previous sampling does not only select cloudy points in the vertical layers where clouds exist. Therefore, a supplementary condition on the existence of liquid water content is added above $z = z_b + (z_t - z_b)/4$ to ensure that above that level only cloudy points are selected. This level is chosen since it corresponds to the level where the selection of non-cloudy points is minimum, ensuring vertical continuity. This condition was not directly added at cloud base to allow the selection of overshooting dry thermals. This addition induces modification in the upper half of clouds as shown in Fig. 6 with vertical profiles of thermal characteristics in-between the cloud and core sampling profiles as illustrated for w. It also induces a larger contribution to the liquid potential temperature and total moisture fluxes in the upper part of the cloud layer, consistent with the core sampling. The cloudy air not selected by this new sampling corresponds to, (i) cloudy air with a small concentration of tracer (5% in the upper part to 15% in the lower part of the cloud layer), (ii) cloudy downdrafts (with more downdrafts in the upper half than lower half of the cloud layer as indicated previously). This choice is quite arbitrary and may deserve further considerations.

4.6 Benefits of the use of a Tracer Instead of the Total Water

Figure 7 shows differences between samplings based on r_t (grey) and two tracers with different lifetimes (15 min for sv, black, and 1 h for sv_2, dark grey dash-dot-dot lines). Coverage fractions are very similar in the cloudy region partly due to the constraint on the liquid water content. In the sub-cloud layer, the samplings based on the two tracers slightly differ: that with a longer lifetime has a vertical profile closer to the r_t sampling profile. The striking difference is the vertical decrease followed by an increase of the coverage fraction in the r_t sampling whereas the coverage fraction mainly decreases for the tracer samplings. This is related to the shape of the r_t variance used as a threshold (using a threshold of zero gives similar results between the tracer and r_t), and reflects the large mixing of r_t by coherent structures in the CBL. This is not the case for the tracer, which is destroyed with a certain lifetime. In fact, the sv short lifetime induces a very small concentration in the environment and therefore ensures that only the active thermals, departed from the surface recently, are selected. The tracer deposited by previous thermals rapidly disappears due to the radioactive decay. Despite these relatively large differences in the coverage fraction, there are only small differences in thermodynamic characteristics of thermals as tracer concentration has a similar behaviour to r_t: it is transported upward. Figure 7 also presents the contribution to the liquid potential temperature and total moisture fluxes of those different conditional samplings. The conditional sampling is the one that has the largest contribution, justifying the choice of considering sv instead of r_t. Note that in the lower part of the cloud layer, sv or r_t samplings

have a larger contribution to the flux than the cloud and core samplings, emphasizing the role of overshooting thermals that need to be accounted for in the transition zone. For information, the sampling using 5% percentiles of the highest values of w as proposed by Siebesma et al. (2007) is also presented in Fig. 7 (light grey dotted line). As expected, this criterion is not adapted in the cloud layer especially in the upper part of the cloud layer (constant coverage fraction, decreasing θ_l anomaly in the upper part of the cloud layer). Moreover, in the sub-cloud layer, its contribution to the total turbulent fluxes is smaller.

5 Contribution to Fluxes and Variances of the Conditional Sampling Structures

With such a sampling, it is possible to quantify the contribution of coherent structures to the vertical transport. In the following, we distinguish the contribution of the structures (organized turbulence as expressed by a top-hat representation, first right-hand side (r.h.s.) in Eq. 4), of the environment (second r.h.s.) and of the in-structure variability (i.e. both the inter-thermal and intra-thermal variability , third r.h.s.) (see Siebesma and Cuijpers 1995):

$$\overline{a'b'} = \alpha(1-\alpha)(a_u - a_e)(b_u - b_e) + (1-\alpha)\overline{a'b'}^e + \alpha\overline{a'b'}^u. \tag{4}$$

The 'u' subscript refers to the average over thermals and the 'e' subscript to the average over the environment. The overbar indexed u (e) denotes a thermal (environmental) average of the fluctuations, those fluctuations being defined with respect to the thermal (environmental) average. α is the coverage fraction of thermals. A mass-flux scheme treats the organized turbulence term; the other two terms are accounted for by an eddy-diffusivity scheme.

Figures 8 and 9 show the contribution of sampled structures to respectively liquid potential temperature and moisture fluxes and variances. In the cloud layer, coherent structures (sampled by the conditional sampling, dotted lines) are responsible for almost 100% of the vertical turbulent flux as illustrated in Figs. 8 and 9 for the liquid potential temperature and moisture fluxes. The addition of the cloud condition does not modify the contribution to the turbulent transport except at the top of clouds (not shown). This correct representation in the cloud layer was already shown by Siebesma and Cuijpers (1995) for the core sampling. Yet, the core sampled structures underestimate the fluxes near cloud base whereas the conditional sampling structures correctly represent the total flux in the transition zone from the sub-cloud to the cloud layer. In the sub-cloud layer, the coherent structures explain about 50–60% in the lower part, and about 60–80% for the moisture flux and 70–90% for the liquid potential temperature flux in the upper part of the sub-cloud layer. For the moisture flux, this is partly due to the strong contribution of the dry tongues, identified by descending dry air ($r_t' < -\sigma_{r_t}$ and $w < 0$) as already shown by Couvreux et al. (2005, 2007). Dry tongues have a smaller impact on the liquid potential temperature flux even though they are responsible for a small vertical shift of the flux up to the cloud base. Small-scale processes also contribute to fluxes as shown by Siebesma et al. (2007) emphasizing the relevance of combining an eddy-diffusivity scheme with a mass-flux scheme.

This sampling can also be used to analyze the contribution of coherent structures to variances. As shown by Wang and Stevens (2000), the top-hat representation fails to simulate the complete variance due to the equal contribution of each fluctuation, implying a strong contribution of small-scale processes. This was also previously demonstrated based on theoretical grounds assuming jointly Gaussian distributions of w and scalars by Wyngaard and Moeng (1992). Only about 30–40% of the variance is accounted for by the coherent structures in the sub-cloud and cloud layer (Figs. 8, 9). These results hold for the various cases and the

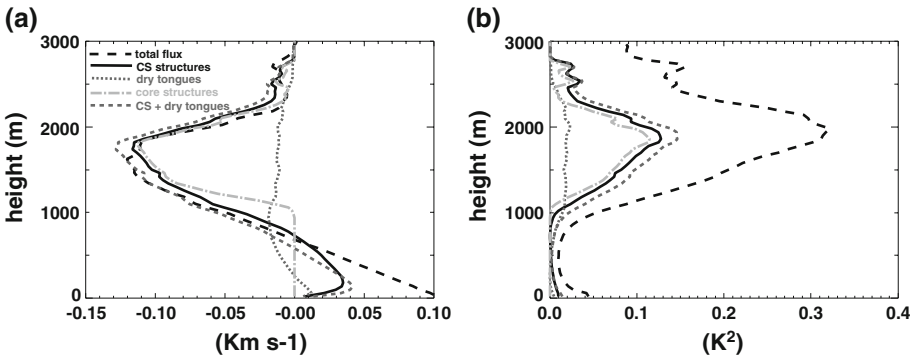

Fig. 8 Contribution to liquid potential temperature **a** flux and **b** variance of the CS structures (*black line*), the dry tongues (*dotted dark grey line*) and the core structures (*dash-dot light grey line*) for ARM 1430 LT. The *long-dashed black* (respectively *dashed dark-grey*) lines corresponds to the total flux or variance (resp. the sum of the contribution of the CS and the dry tongues)

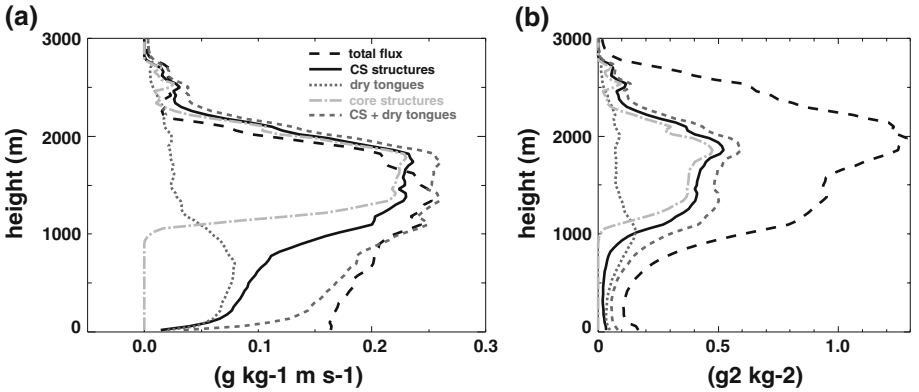

Fig. 9 Contribution to total water vapour mixing ratio **a** flux and **b** variance of the CS structures (*black line*), the dry tongues (*dotted dark grey line*) and the core structures (*dash-dotted light grey line*) for ARM 1430 LT. The *long-dashed black* (respectively *dashed dark-grey*) lines corresponds to the total flux or variance (resp. the sum of the contribution of the CS and the dry tongues)

different times. The dry tongues also significantly contribute to the moisture variance as shown in Fig. 9.

Using the conditional sampling, we have determined here the contribution to fluxes and variances of thermals from the surface to the top of the cloud layer and therefore complemented the study of Wang and Stevens (2000). It highlights that thermals explain most of the fluxes in the cloud layer and (although to a lesser extent) in the sub-cloud layer. Nevertheless, conditional sampling suggests potential future improvements for boundary-layer schemes by taking into account the entrainment structures that are also coherent structures as suggested by Couvreux et al. (2007) and improving the representation of small-scale variability. In particular, the latter is necessary when the variance is used to diagnose the cloud cover.

6 Conclusion

In the present study, we addressed the question of the design of a conditional sampling on LES results well suited for the evaluation and improvement of CBL mass-flux parametrizations. We defined a conditional sampling that explains the largest fraction of the turbulent vertical flux of large-scale conserved variables (like θ_l and r_t), but with the smallest fraction of the domain in order to only select the convective plumes accounted for by the mass-flux schemes.

For the first time to our knowledge, a conditional sampling that characterizes thermals continuously from the surface to the top of the dry or cloudy boundary layers in LES is proposed. This sampling characterizes the bottom-up transport and is based on the use of a tracer emitted at the surface with a lifetime of a fraction of hour. Its ability to select thermals is evaluated for cloud-free and cloudy boundary layers against observations and more traditional conditional samplings (the θ_v sampling up to $0.8z_i$ and the cloud and core samplings). The new sampling enables us to describe the transition zone from the sub-cloud to the cloud layer. Moreover, it explains similar contribution to fluxes than given by a buoyancy sampling in the lower part of the boundary layer, and than given by a cloud/core sampling in the cloudy part. The sampling is done with a 1σ threshold on the tracer, which is shown to give the smallest coverage fraction with no reduction of the total flux accounted for (with respect to a less restrictive sampling).

This new conditional sampling is used in Part II of our study (Rio et al. 2010) to evaluate and improve a boundary-layer thermal parametrization, the thermal plume model of Rio and Hourdin (2008). In particular, it is used to validate a new formulation for fractional entrainment and detrainment rates.

The new conditional sampling relies on a virtual tracer. For links with observations or as a practicable alternative for model evaluation, total water can be used instead. The virtual potential temperature is also adapted for studies focusing only on the lower part of the boundary layer. When radar images are available, they can also be used directly for sampling, since radar echoes are sensitive to insects coming from the surface, which play a role similar to our passive tracer. Similar remarks probably hold for aerosol Lidar observations.

The new conditional sampling accounts for a very large fraction of the liquid potential temperature flux above cloud base. Below $0.6z_i$, it accounts for only 50–60%, but the other 40–50% is due to small-scale non-organized structures that are not intended to be represented by the mass-flux scheme, but rather by turbulent diffusion approaches. This demonstrates that the combination of an appropriate mass-flux parametrization of the buoyant convective structures with turbulent diffusion should be able to properly represent the liquid potential temperature flux.

The situation is a little different for total water, for which the dry tongues (coherent structures of dry air descending from the free troposphere into the CBL, Couvreux et al. (2007)) are responsible for a significant part of the flux up to the cloud base. Note that the dry tongues are also responsible for a small vertical shift of the total flux of liquid potential temperature in the transition zone. These dry tongues may thus require further development of the mass-flux parametrization in the future.

If needed, a good representation of the variance for one particular variable requires an additional parametrization for the sub-structure or intra-structure variance, which explains more than half of the total variance.

References

Albrecht BA (1981) Parameterization of trade-cumulus cloud amounts. J Atmos Sci 38:97–105

Atkinson BW, Zhang JW (1996) Mesoscale shallow convection in the atmosphere. Rev Geophys 34:403–431

Berg L, Stull RB (2004) Parameterization of joint frequency distributions of potential temperature and water vapor mixing ratio in the daytime convective boundary layer. J Atmos Sci 61:813–828

Brown AR, Cederwall RT, Chlond A, Duynkerke PG, Golaz M, Khairoutdinov JC, Lewellen DC, Lock AP, Macvean MK, Moeng CH, Neggers RAJ, Siebesma AP, Stevens B (2002) Large-eddy simulation of the diurnal cycle of shallow cumulus convection over land. Q J Roy Meteorol Soc 128:1075–1093

Chatfield RB, Brost RA (1987) A two-stream model of the vertical transport of trace species in the convective boundary layer. J Geophys Res 92:13263–13276

Couvreux F, Guichard F, Redelsperger J-L, Kiemle C, Masson V, Lafore J-P, Flamant C (2005) Assessment of water vapour variability within a convective boundary layer over land using large eddy simulations and ihop observations. Q J Roy Meteorol Soc 131:2665–2693

Couvreux F, Guichard F, Masson V, Redelsperger J-L (2007) Negative water vapour skewness and dry tongues in the convective boundary layer: observations and les budget analysis. Boundary-Layer Meteorol 123:269–294

Crum TD, Stull RB, Eloranta EW (1987) Coincident lidar and aircraft observations of entrainment into thermals and mixed layers. J Clim Appl Meteorol 26:774–788

Cuxart J, Bougeault P, Redelsperger J-L (2000) A turbulence scheme allowing for mesoscale and large-eddy simulations. Q J Roy Meteorol Soc 126:1–30

Greenhut GK, Khalsa SJS (1982) Updraft and downdraft events in the atmospheric boundary layer over the equatorial pacific ocean. J Atmos Sci 39:1803–1817

Grossman RL (1984) Bivariate conditional sampling of moisture flux over a tropical ocean. J Atmos Sci 41:3238–3253

Heus T, Jonker HJJ (2008) Subsiding shells around cumulus clouds. J Atmos Sci 65:1003–1018

Hourdin F, Couvreux F, Menut L (2002) Parameterization of the dry convective boundary layer based on a mass flux representation of thermals. J Atmos Sci 59:1105–1123

Lafore J-P, Stein J, Ascencio N, Bougeault P, Ducrocq V, Duron J, Fischer C, Hereil P, Mascart P, Masson V, Pinty J-P, Redelsperger J-L, Richard E, Vil-Gueraude de Arellano J (1998) The meso-nh atmospheric simulation system. Part i: Adiabatic formulation and control simulations. Ann Geophys 16:90–109

LeMone MA, Pennell WT (1976) The relationship of trade wind cumulus distribution to subcloud layer fluxes and structure. Mon Weather Rev 104:524–539

Lenschow DH, Stephens PL (1980) The role of thermals in the convective boundary layer. Boundary-Layer Meteorol 19:509–532

Lenschow DH, Wyngaard JC, Pennel WT (1980) Mean-field and second-moment budgets in a baroclinic, convective boundary layer. J Atmos Sci 37:1313–1326

Miao Q, Geerts B, Lemone M (2006) Vertical velocity and buoyancy characteristics of coherent echo plumes in the convective boundary layer, detected by a profiling airborne radar. J Appl Meteorol Clim 45:838–855

Moeng C, Sullivan PP (1994) A comparison of shear- and buoyancy-driven planetary boundary layer flows. J Atmos Sci 51:999–1022

Nicholls S, LeMone MA (1980) Fair weather boundary layer in GATE: the relationship of subcloud fluxes and structure to the distribution and enhancement of cumulus clouds. J Atmos Sci 37:2051–2067

Pergaud J, Masson V, Malardel S, Couvreux F (2009) A parameterization of dry thermals and shallow cumuli for mesoscale numerical weather prediction. Boundary-Layer Meteorol 132:83–106. doi:10.1007/s10546-009-9388-0

Rio C, Hourdin F (2008) A thermal plume model for the convective boundary layer: representation of cumulus clouds. J Atmos Sci 65:407–425

Rio C, Couvreux F, Hourdin F (2010) Resolved versus parametrized boundary-layer plumes. Part II: A new formulation of mixing rates for mass-flux schemes. Boundary-Layer Meteorol (under review)

Schumann U, Moeng C-H (1991) Plume fluxes in clear and cloudy convective boundary layers. J Atmos Sci 48:1746–1757

Siebesma AP, Cuijpers JWM (1995) Evaluation of parametric assumptions for shallow cumulus convection. J Atmos Sci 52:650–666

Siebesma AP, Teixeira J (2000) An advection-diffusion scheme for the convective boundary layer: description and 1d-results. In: Proceedings of the 14th symposium on boundary layers and turbulence, Aspen, CO, American Meteorological Society, pp 133–136

Siebesma AP, Bretherton CS, Brown A, Chlond A, Cuxart J, Duynkerke PG, Jiang H, Khairoutdinov M, Lewellen D, Moeng C-H, Sanchez E, Stevens B, Stevens DE (2003) A large eddy simulation intercomparison study of shallow cumulus convection. J Atmos Sci 60:1201–1219

Siebesma AP, Soares PMM, Teixeira J (2007) A combined eddy-diffusivity mass-flux approach for the convective boundary layer. J Atmos Sci 64:1230–1248

Soares PMM, Miranda PMA, Siebesma AP, Teixeira J (2004) An eddy-diffusivity/mass-flux parameterization for dry and shallow cumulus convection. Q J Roy Meteorol Soc 130:3365–3383

Sorbjan Z (1986) On similarity in the atmospheric boundary layer. Boundary-Layer Meteorol 34:377–397

Wang S, Stevens B (2000) Top-hat representation of turbulence statistics in cloud-topped boundary layers: a large-eddy simulation study. J Atmos Sci 57:423–441

Weckwerth TM, Parsons DB, Koch SE, Moore JA, LeMone MA, Demoz BB, Flamant C, Geerts B, Wang J, Feltz WF (2004) An overview of the international h20 project ($IHOP_{2002}$) and some preliminary highlights. Bull Am Meteorol Soc 85:253–277

Williams AG, Hacker JM (1992) The composite shape and structure of coherent eddies in the convective boundary layer. Boundary-Layer Meteorol 61:213–245

Wyngaard JC, Moeng C-H (1992) Parameterizing turbulent diffusion through the joint probability density. Boundary-Layer Meteorol 60:1–13

Young GS (1988) Turbulence structure of the convective boundary layer. Part II: Phoenix 78 aircraft observations of thermals and their environment. J Atmos Sci 45:727–735

Zhao M, Austin PH (2005) Life cycle of numerically simulated shallow cumulus clouds. Part I: Transport. J Atmos Sci 62:1269–1290